*Korean J. of Chem. Eng.*, **13**(2), 105-114 (1996)

# DEPOSITION UNIFORMITIES ON A WAFER AND IN A TRENCH FOR TUNGSTEN SILICIDE LPCVD IN A SINGLE-WAFER REACTOR

**Jung-Hwan Park**

Dept. of Chemical, Bio & Materials Engineering and, Center for Solid State Electronics Research,
Arizona State University, Tempe, AZ 85287-6006
*(Received 27 September 1994 • accepted 1 November 1996)*

**Abstract**—A transient model of a single-wafer reactor in axisymmetric, stagnation point flow is used to study the effects of operating conditions on film thickness uniformity and composition uniformity across the wafer during low pressure chemical vapor deposition of tungsten silicide. Orthogonal collocation on finite elements is used to solve the transient model equations; continuity, momentum, energy and chemical species balances. A feature scale model for simultaneous Knudsen transport and heterogeneous reactions is used to predict film thickness in infinite trenches. Boundary conditions for the feature scale model are established using the reactor scale model. The use of a combined reactor scale and feature scale model is demonstrated to select deposition conditions which provide both good interwafer uniformity and good intrafeature uniformity. Film thickness and composition uniformity on a wafer are predicted using a model for a single-wafer reactor. Significant differences in step coverage predicted using partial pressures in the feed stream and partial pressures at the wafer surface were observed. Step coverage differences between the wafer center and the wafer edge were also significant under the operating conditions used in this study. Uniformities of interwafer and intrafeature step coverages inceased as either the wafer temperature or the partial pressure ratio of dichlorosilane to tungsten silicide in the feed was decreased.

*Key words: Deposition Uniformity, Step Coverage, Chemical Vapor Deposition, Single-Wafer Reactor, Tungsten Silicide*

## INTRODUCTION

Film thickness and composition (where applicable) uniformity across a wafer as well as in features on patterned wafers are critical film properties in microelectronics applications. Trends toward large diameter silicon wafers [Bullis and O'Mara, 1993] particularly when combined with decreasing dimensions in integrated circuits, make these demands become more stringent [Moslehi et al., 1992]. Single-wafer reactors (SWRs) are often preferred to conventional volume loaded multiple wafer reactors (MWRs), because they offer the possibility of superior deposition uniformity at high conversion levels of costly reactants. SWRs also provide other advantages over MWRs such as; easier automatic wafer handling, easier adjustment of process variations, higher wafer-to-wafer consistency and lower capital cost [Moslehi et al., 1992; Lam and Koch, 1980]. Another important advantage of SWRs over MWRs is that process upsets will result in misprocessing of only one wafer instead of an entire batch. Interest in SWRs has grown recently for chemical vapor deposition (CVD) processes [Kleijn et al., 1989; Jasinski and Kang, 1991; Rode and Schmitz, 1992; Dobskin, 1992; Cale et al., 1993], for etching processes [Economou and Alkire, 1988; Park and Economou, 1990; Riely and Clark, 1991] and for rapid thermal processing [Wong, 1989; Campbell et al., 1990; Chatterjee et al., 1992]. On the other hand, SWRs present new challenges to the process engineer. Higher deposition rates are required for an SWR, since device throughput must be competitive with that of a conventional MWR. Unfortunately, as deposition rate increases, film conformality in patterned regions of the wafer tends to degrade. Increasing temperature and/or reactant partial pressure will generally increase deposition rates; however, this may lead to gas phase reactions, lower deposition uniformity across wafer and poorer film conformality in features. Therefore, it is critical to know how operating conditions impact uniformity of the deposited films across a wafer as well as in features on patterned wafers.

A reactor scale model (RSM) for low pressure chemical vapor deposition (LPCVD) SWRs of an impinging jet type has been presented by Kleijn et al. [1989] for silicon deposition from silane. Their model incorporates multicomponent diffusion, thermodiffusion, and variable gas properties. Homogeneous reactions and the Dufour effect were not included. Their model was refined with inclusion of the Dufour effect for tungsten deposition by the hydrogen reduction of tungsten hexafluoride [Kleijn et al., 1991] and with inclusion of gas phase reactions for silicon deposition from silane [Kleijn, 1991]. In this work, a transient RSM of a stagnation point flow SWR is used, which has been used to study the inherent transients which occur during deposition processes [Cale et al., 1991a, 1992a, b, 1993]. Our model includes multicomponent diffusion, thermal diffusion, multiple surface reactions, the Dufour effect and variable gas properties. The RSM is solved with given boundary conditions to predict the velocity, temperature, and chemical species concentration fields within the SWR. Reactant concentrations and perhaps the temperature at the wafer surface are computed as part of the solution, and these are used as boundary conditions for the feature scale model to predict step coverage in trenches on patterned wafers. Computation of local wafer temperatures are considerably complicated and has been perform-

†Present address: Dept. of Environmental Engineering, Junior College of Inchon, 235, Dohwa-dong, Nam-gu, Inchon

ed using the wafer energy balance [Ulacia et al., 1989; Park, 1992]. The wafer temperature, however, is considered as constant in this study.

Two distinct approaches, continuum-like diffusion reaction model (DRM) [McConica et al., 1988; Raupp and Cale, 1989; Chatterjee and McConica, 1990; Cale et al., 1990] and ballistic transport and reaction model (BTRM) [Cale and Raupp, 1990; Cale et al., 1991b; IslamRaja et al., 1991], have been presented to predict step coverage in features. Qualitative trends in film conformality with changes in operating conditions were observed by the two models [Jain et al., 1993]. Quantitative agreement between predicted and experimental step coverages can be achieved if the reaction kinetics and the local deposition conditions are accurately known. For LPCVD systems, much of the existing disagreement between experimental and simulated film profiles is believed to be due to uncertainties in the reactant partial pressures at the wafer surface and perhaps the wafer temperature. These deposition conditions are primary variables which determine step coverage and film composition. In the case of cold wall SWRs where deposition rates must be high in order to obtain high throughput and reactor walls are cooled, the reactant concentrations at the reactor inlet can be much higher than their concentrations calculated at the wafer surface, because of high conversion levels of the gaseous reactants. Even in the case of low reactant conversion levels, the concentrations in the feed stream may not represent those at the wafer surface due to byproduct generation and thermal diffusion effects. Local deposition conditions at the wafer surface can be predicted by a validated RSM, when there are no direct measurements of gas phase composition during deposition. The DRM is used in this paper, since it is formulated in terms of transient differential equations and is therefore more consistent with the RSM used than the integro-differential equations of the BTRM. The RSM has been combined with both the DRM and the BTRM for estimating film conformality in infinite trenches on the wafer [Cale et al., 1993].

The overall goal of this paper is to demonstrate the use of a combined reactor scale and feature scale model to gain insight into LPCVD processes. More importantly, an attention is focused on the possibilities of having thickness, composition and step coverage uniformities across a wafer. The RSM is used to predict film thickness and composition uniformity on the wafer. The DRM is simultaneously used to predict step coverage in a trench.

## TUNGSTEN SILICIDE LPCVD CHEMISTRY

Tungsten silicide deposition by the dichlorosilane (DCS) reduction of tungsten hexafluoride is considered. Tungsten silicide appears to be an excellent candidate material for interconnect applications. Three deposition reactions which form the three different phases were proposed [Raupp et al., 1990] in films deposited in a range of conditions which includes the conditions in the present study. The stoichiometric equations used are

$$\text{I. } SiH_2Cl_2 \rightarrow Si + 2HCl \tag{1}$$

$$\text{II. } WF_6 + 4SiH_2Cl_2 \rightarrow WSi_2 + 8HCl + SiF_4 + SiF_2 \tag{2}$$

$$\text{III. } 5WF_6 + 11SiH_2Cl_2 \rightarrow W_5Si_3 + 22HCl + 7SiF_4 + SiF_2. \tag{3}$$

The surface reaction rates are expressed in terms of the following generic form

$$\Re_j = k_{oj}\exp\left(-\frac{E_{aj}}{R_gT}\right)\left(\frac{P_{DCS}^{\alpha_j}p_{WF_6}^{\beta_j}}{1+K_jp_{WF_6}}\right) \quad j = Si,\ WSi_2,\ W_5Si_3 \tag{4}$$

**Table 1. Kinetic parameters for $WSi_x$ deposition**

| Solid j | $k_0$ [mol/(cm² s torr$^{(\alpha+\beta)}$)] | $E_a$ (kcal/mol) | $\alpha$ | $\beta$ | K (torr$^{-1}$) |
|---|---|---|---|---|---|
| Si | 6.6E22 | 90 | 2 | 0 | 0 |
| $WSi_2$ | 1.8E30 | 120 | 1 | 1 | 1 |
| $W_5Si_3$ | 8.3E4 | 40 | 0.5 | 1 | 0 |

where $p_{DCS}$ and $p_{WF_6}$ are the partial pressures of DCS and $WF_6$ in torr, respectively. $k_{oj}$ and $E_{aj}$ are the pre-exponential factor and activation energy respectively for reaction j. $\alpha_j$ and $\beta_j$ are the reaction order in DCS and $WF_6$ respectively, and $K_j$ is the absorption coefficient of $WF_6$ for reaction j. The reaction rate is in gmole/cm² sec. The values of the parameters for each reaction are given in Table 1 [Cale et al., 1991a]. These values were determined over a range of temperature and reactant partial pressures which includes the steady state temperature and reactant partial pressures at the wafer surface.

## MATHEMATICAL MODEL FOR A SINGLE-WAFER RACTOR

A comprehensive representation of a CVD reactor requires a set of partial differential equations which consists of a momentum balance, thermal energy balance and species balance equations. The transient SWR model used in this study has a steady state version which is similar to that of Kleijn et al. [1989, 1991]. The mathematical model of the SWR has been described elsewhere [Cale et al., 1993]. In developing the model, the major assumptions used are:

(1) The flow is laminar and axisymmetric.
(2) Gases are ideal.
(3) The fluid behaves as a continuum.
(4) Radiant heat transfer between the solid surfaces is ignored.
(5) Contributions of heat flux from viscous dissipation and pressure changes are ignored.
(6) Gas phase reactions are negligible.
(7) Contributions of mass flux from pressure diffusion and forced diffusion are neglected.
(8) There is no deposition on solid surfaces other than the reactive surfaces.

### 1. Transport Equations

Based on these assumptions, the system can be described by the following governing partial differential equations. Variables and parameters are defined in the List of Symbols.

Continuity equation

$$\frac{\partial\rho}{\partial t} + \nabla\cdot(\rho\mathbf{v}) = 0 \tag{5}$$

Momentum balance

$$\frac{\partial}{\partial t}(\rho\mathbf{v}) = -\nabla\cdot(\rho\mathbf{v}\mathbf{v}) + \nabla\cdot\left[\mu_m\{\nabla\mathbf{v} + (\nabla\mathbf{v})^t\} - \frac{2}{3}\mu_m(\nabla\cdot\mathbf{v})\cdot\mathbf{I}\right] - \nabla P + \rho\mathbf{g} \tag{6}$$

Energy balance

$$\frac{\partial}{\partial t}(\rho c_{pm}T) = -\nabla\cdot(\rho c_{pm}\mathbf{v}T) + \nabla\cdot(\lambda_m\nabla T) + \nabla\cdot\left[R_gT\sum_{i=1}^{n}\frac{D_i^T}{m_i}\nabla(\ln x_i)\right] \tag{7}$$

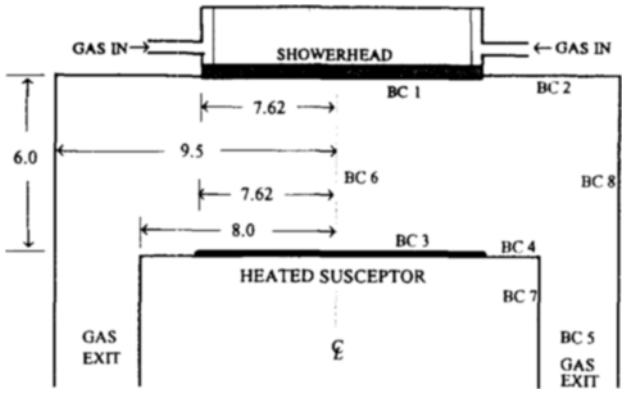


**Fig. 1. Schematic of single-wafer reactor, along with reactor dimensions. BC number indicates the surface on which the boundary conditions are applied.**

Species balance

$$\frac{\partial}{\partial t}(\rho\omega_i) = -\nabla\cdot(\rho v\omega_i) + \nabla\cdot(\rho D_{im}\nabla\omega_i) + \nabla\cdot[D_i^T\nabla(\ln T)]. \quad (8)$$

There are $n$-1 independent species balance equations, with the composition of the $n$th species determined using the constraint the sum of the mass fractions is one. The last term in bracket of Eq. (8) represents the thermal diffusion (Soret effect) which occurs when gas molecules experience a driving force due to temperature gradients. This effect is usually insignificant compared to ordinary diffusion. However, the Soret effect can play a significant role in cold wall reactors due to both steep temperature gradients near the hot susceptor and differences in molecular weights among gaseous components. In the presence of temperature gradients, the heavier and larger molecules tend to concentrate in the colder regions, whereas the lighter and smaller molecules move towards the hotter regions. The last term of Eq. (7) represents the Dufour energy flux resulting from concentration gradients, which is the reciprocal process to thermal diffusion.

The density of the gas mixture is calculated by the equation of state using the species mass fraction and its molecular weight

$$\rho = \frac{P}{R_g T}\sum_{i=1}^{n}\frac{\omega_i}{\sum_{j=1}^{n}\omega_j/m_j}. \quad (9)$$

## 2. Boundary Conditions and Initial Conditions

The boundary conditions on the SWR are the following, where the number refers to the position of the reactor shown in Fig. 1, along with the configuration of the reactor

$$\text{BC 1: } v_r=0,\ v_z=v_0,\ T=T_0,\ \omega_i=\omega_{i,0} \quad (10)$$

$$\text{BC 2: } v_r=0,\ v_z=0,\ T=T_w,\ \rho D_{im}\frac{\partial\omega_i}{\partial z}+D_i^T\frac{\partial}{\partial z}(\ln T)=0 \quad (11)$$

$$\text{BC 3: } v_r=0,\ v_z=-\frac{1}{\rho}\sum_{i=1}^{n}m_i\sum_{j=1}^{l}\nu_{ij}\Re_j,\ T=T_s,$$
$$\rho D_{im}\frac{\partial\omega_i}{\partial z}+D_i^T\frac{\partial}{\partial z}(\ln T)=m_i\sum_{j=1}^{l}\nu_{ij}\Re_j \quad (12)$$

$$\text{BC 4: } v_r=0,\ v_z=-\frac{1}{\rho}\sum_{i=1}^{n}m_i\sum_{j=1}^{l}\nu_{ij}\Re_j,\ \frac{\partial T}{\partial z}=0,$$
$$\rho D_{im}\frac{\partial\omega_i}{\partial z}+D_i^T\frac{\partial}{\partial z}(\ln T)=m_i\sum_{j=1}^{l}\nu_{ij}\Re_j \quad (13)$$

$$\text{BC 5: } v_r=0,\ \frac{\partial v_z}{\partial z}=0,\ \frac{\partial T}{\partial z}=0,\ \frac{\partial\omega_i}{\partial z}=0 \quad (14)$$

$$\text{BC 6: } v_r=0,\ \frac{\partial v_z}{\partial r}=0,\ \frac{\partial T}{\partial r}=0,\ \frac{\partial\omega_i}{\partial r}=0 \quad (15)$$

$$\text{BC 7: } v_r=0,\ v_z=0,\ \frac{\partial T}{\partial r}=0,\ \rho D_{im}\frac{\partial\omega_i}{\partial r}+D_i^T\frac{\partial}{\partial r}(\ln T)=0 \quad (16)$$

$$\text{BC 8: } v_r=0,\ v_z=0,\ T=T_w,\ \rho D_{im}\frac{\partial\omega_i}{\partial r}+D_i^T\frac{\partial}{\partial r}(\ln T)=0. \quad (17)$$

It is noted that a uniform gas velocity is used at the reactor inlet. The use of plug flow is quite reasonable for the showerhead rather than the use of well developed flow [Fitzjohn and Holstein, 1990]. There is a finite normal velocity component at the reactive surfaces because of the surface reactions. On the reactive surfaces, the net mass flux normal to the surface equals the rate of surface reactions, as indicated in Eq. (12). The local film growth rate in Angstrom/min, in terms of the sum of the surface reactions, is

$$F=\left(\sum_{j=1}^{3}\frac{m_{sj}}{\rho_{sj}}\Re_j\right)60\times10^8 \quad (18)$$

where $m_{sj}$ is the molecular mass of solid species produced by reaction j, and $\rho_{sj}$ is its density. The silicon to tungsten ratio in the deposited film is calculated by the ratio of reaction rates

$$\frac{Si}{W}=\frac{\Re_1+2\Re_2+3\Re_3}{\Re_2+5\Re_3}. \quad (19)$$

In addition, the total pressure is specified at the reactor outlet, where it is often measured in practice.

The appropriate initial conditions depend how the process runs. The susceptor temperature can be ramped up after the reactant flow rates have been established or *vice versa*. These startup transients have been studied [Cale et al., 1991a, 1992a]. However, these transients are ignored in this paper and calculations focus on steady state predictions even though the transient equations are used to solve a set of partial differential equations of the SWR.

## 3. Transport Coefficients

The transport coefficients for the gas mixture are functions of temperature, pressure and composition of the gas mixture. The calculation of transport properties is based on the Chapman-Enskog theory and on the Lennard-Jones 6-12 potentials [Reid et al., 1988; Hirschfelder et al., 1954]. The heat capacity of gaseous species in this system is available [Chase et al., 1985; Pankratz, 1984]. A detailed computation of transport coefficients is described in Appendix. For computation, local values for transport coefficients are calculated at local temperature, pressure and concentration in the gas phase.

## 4. Numerical Solution

Orthogonal collocation on finite elements (OCFE) with Lagrange polynomials is used to solve the set of transient partial differential equations. This approach is a method of weighted residuals and is very attractive in terms of the required computational effort and accuracy [Finlayson, 1980; Suwondo et al., 1991]. In OCFE, the solution domain is divided into many discrete rectangular subdomains which fill the entire spatial region. The axisymmetric half of the cylindrical domain is discretized on a nonuniform grid, which consists of 31 nodes in the axial direction and 28 nodes in the radial direction. The use of OCFE removes the spa-

tial derivatives, converting the set of nonlinear partial differential equations to a set of nonlinear ordinary differential equations (ODEs) in time. The set of nonlinear ODEs along with algebraic equations resulting from the boundary conditions can be readily solved using subroutine DVODE which is available from ode library at AT&T Bell Labs [Netlib]. The initial values for the dependent variables at each point are determined under no reaction conditions by solving the steady state of momentum and energy balance equations using subroutine HYBRD which is the nonlinear equation solver taken from *minpack* library at AT&T. The reason for calculation of initial advance is that deposition processes commonly used in the microelectronic devices run with inert gas until establishing fully developed velocity and susceptor temperature in the reactor, as mentioned early in this section.

## MATHEMATICAL MODEL IN A TRENCH

Consider deposition in a long trench on a patterned wafer. A one-dimensional continuum-like formulation is used in which molecular transport is described by cross sectional averaged Knudsen diffusion and deposition by classical heterogeneous reaction rate expressions. In order to develop a mathematical model for the LPCVD system in a trench, the following assumptions [Cale et al., 1993] are made:

(1) The mass transfer within the trench is prevailed by Knudsen diffusion or free molecular flow.

(2) Lateral concentration gradients in the trench are assumed to be negligible.

(3) Surface diffusion is insignificant.

(4) The open end of the trench is exposed to an ideal gas.

(5) The feature is spatially isothermal.

Based on these assumptions and given the stoichiometries, kinetic expressions and trench dimensions, two species balances are required, one for DCS (C) and one for $WF_6$ (F). Choosing DCS as reference species, the dimensionless model equations are

Dichlorosilane Balance

$$\frac{\partial\theta_C}{\partial\tau}=\frac{1}{WH^2}\frac{\partial}{\partial\xi}\left(W\mathcal{B}_C\frac{\partial\theta_C}{\partial\xi}\right)-\frac{1}{W}\left[\left(1-\frac{\theta_C}{\delta_1}\right)\phi_1G_1+\left(4-\frac{\theta_C}{\delta_2}\right)\phi_2G_2+\left(11-\frac{\theta_C}{\delta_3}\right)\phi_3G_3\right] \quad (20)$$

Tungsten Hexafluoride Balance

$$\frac{\partial\theta_F}{\partial\tau}=\frac{\Gamma}{WH^2}\frac{\partial}{\partial\xi}\left(W\mathcal{B}_F\frac{\partial\theta_F}{\partial\xi}\right)-\frac{1}{W}\left[-\frac{\theta_F}{\delta_1}\phi_1G_1+\left(\Lambda_{CF}-\frac{\theta_F}{\delta_2}\right)\phi_2G_2+\left(5\Lambda_{CF}-\frac{\theta_F}{\delta_3}\right)\phi_3G_3\right] \quad (21)$$

In the above mass balance equations, the first term in the right hand side represents the ordinary diffusion flux due to concentration gradient and the second term represents the net reaction rate associated with three surface reactions. Variables and parameters are defined in the List of Symbols.

Boundary Conditions

$$\theta_j(0,\ \tau)=1 \text{ for } \tau>0 \text{ j=C, F} \quad (22)$$

$$\frac{\partial\theta_C(1,\ \tau)}{\partial\tau}=\frac{-1}{2\alpha_0}\frac{H(\tau)}{\mathcal{B}_C(1,\ \tau)}[\phi_1G_1(1,\ \tau)+4\phi_2G_2(1,\ \tau)+11\phi_3G_3(1,\ \tau)] \text{ for } \tau>0 \quad (23)$$

$$\frac{\partial\theta_F(1,\ \tau)}{\partial\tau}=-\frac{\Theta}{2\alpha_0}\frac{H(\tau)}{\mathcal{B}_F(1,\ \tau)}[\phi_2G_2(1,\ \tau)+5\phi_3G_3(1,\ \tau)] \text{ for } \tau>0 \quad (24)$$

Initial Conditions

$$\theta_j(\xi,\ \tau)=1 \text{ for } 0\le\xi\le1 \text{ j=C, F} \quad (25)$$

Trench Width

$$\frac{\partial W(\xi,\ \tau)}{\partial\tau}=-\left(\frac{\phi_1G_1}{\delta_1}+\frac{\phi_2G_2}{\delta_2}+\frac{\phi_3G_3}{\delta_3}\right) \text{ with } W(\xi,\ 0)=1 \text{ for } 0\le\xi\le1 \quad (26)$$

Trench Height

$$\frac{\partial H(\tau)}{\partial\tau}=\frac{1}{2\alpha_0}\left[\frac{\phi_1}{\delta_1}\{1-G_1(1,\ \tau)\}+\frac{\phi_2}{\delta_2}\{1-G_2(1,\ \tau)\}+\frac{\phi_3}{\delta_3}\{1-G_3(1,\ \tau)\}\right] \text{ with } H(0)=1 \quad (27)$$

In the above equations, the step coverage modulus $\phi$ is defined as a ratio of characteristic deposition rate to a characteristic diffusive transport rate. The step coverage enhances with decreasing the step coverage modulus at a constant value of $\Lambda_{CF}$. $\Lambda_{CF}$ is the partial pressure ratio of dichlorosilane to tungsten hexafluoride. Decreasing this ratio improves step coverage at a constant value of the step coverage modulus. The effects of these parameters on step coverage has been studied [Cale et al., 1990, 1993]. Knudsen diffusivity is estimated as discussed in Appendix.

## RESULTS AND DISCUSSION

The reactor dimensions used in the simulation are listed in Fig. 1. The reactor wall temperatures are assumed to be constant and uniform at 300 K, which is also the assumed temperature of the feed gas. The susceptor temperature is 763 K. The total operating pressure is 0.18 torr. The DCS flow rate is 120 sccm and the $WF_6$ flow rate is 3.8 sccm. The motivation for combined reactor scale and feature scale models has been presented by Cale and coworkers [1993]. Startup and shut down transients are not considered, i.e., it is assumed that the deposition occurs mostly at steady state [Cale et al., 1991a, 1992a]. Figs. 2-5 summarize the steady state results of the RSM calculations. Fig. 2 shows the calculated gas flow vectors which indicate the magnitude and the direction of the local mass velocity in a single-wafer reactor. The axial velocity component has its same value at the reactor inlet due to the use of plug flow which is assumed in the showerhead. The use of showerhead can suppress the recirculation in the SWR [Fitzjohn and Holstein, 1990]. Beyond the susceptor edge the velocity profile is nearly parabolic with a zero radial component. Fig. 3 shows the isotherms in half of the reactor. The Dufour effect did not impact the calculated temperatures for the operating conditions used in this study. This observation is consistent with previous simulation results in LPCVD processes [Jenkinson and Pollard, 1984; Kleijn et al., 1991]. Figs. 4a-4c illustrate contours of the mole fractions of $WF_6$, DCS, and HCl, respectively. The mole fractions of the reactants decrease as the wafer surface is approached due to consumption of the reactant gases resulting from surface reactions. Significant radial concentration gradients exist along the wafer. These radial concentration gradients are more pronounced towards the wafer edge. The Soret effect plays a minor role under the conditions of this simulation. The mole fraction contours of reaction products $SiF_4$ and $SiF_2$

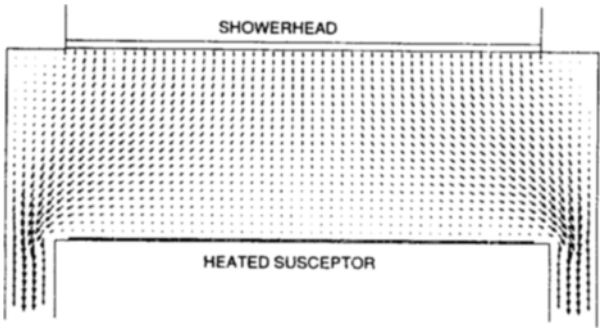


**Fig. 2. Flow velocity vectors in the reactor. The wafer temperature is 763 K, the total pressure is 0.18 torr, the flow rate of DCS is 120 sccm and the flow rate of $WF_6$ is 3.8 sccm.**

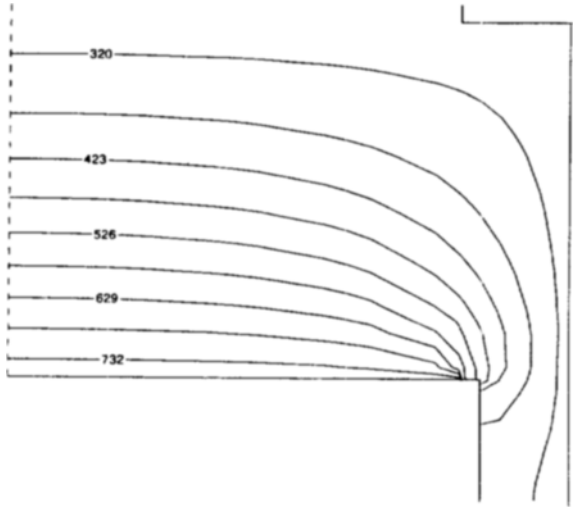


**Fig. 3. Computed isotherms in half of the reactor.**

are not given here but have the same trends as those of HCl. Fig. 5 shows the total deposition rate as a function of wafer radius. The increase in deposition rates with radial position is mostly due to the radial gradients in reactant partial pressures at the wafer surface, as dictated by Eq. (4). Fig. 5 also shows the ratio of deposited silicon to tungsten. This ratio changes by 3.2% across the wafer, even though the deposition rate changes by 13.7%. The reason for small change of Si/W is due to the fact of that the rates of deposition of both silicon and tungsten increase with increasing reaction rates at the wafer surface.

The partial pressures at the wafer surface, computed as part of the solution from the RSM, provide the concentrations of dichlorosilane and $WF_6$ for the DRM. Fig. 6 shows the ratios of DCS to $WF_6$ partial pressures at the wafer surface and ratios of $WF_6$ partial pressure at the wafer surface to $WF_6$ partial pressure in the feed stream as functions of wafer temperature when the other operating conditions are fixed at the values prescribed above. Significant depletion of $WF_6$ occurs for temperature above 770 K. The difference in $WF_6$ depletion between the wafer center and wafer edge increases with increasing temperature, and $WF_6$ depletion at the wafer center becomes much higher than that at the wafer edge at higher temperatures. The partial pressure ratios at the wafer surface $\Lambda_{CF}$ increase as the temperature increases, but the ratios of $WF_6$ partial pressure at the wafer surface

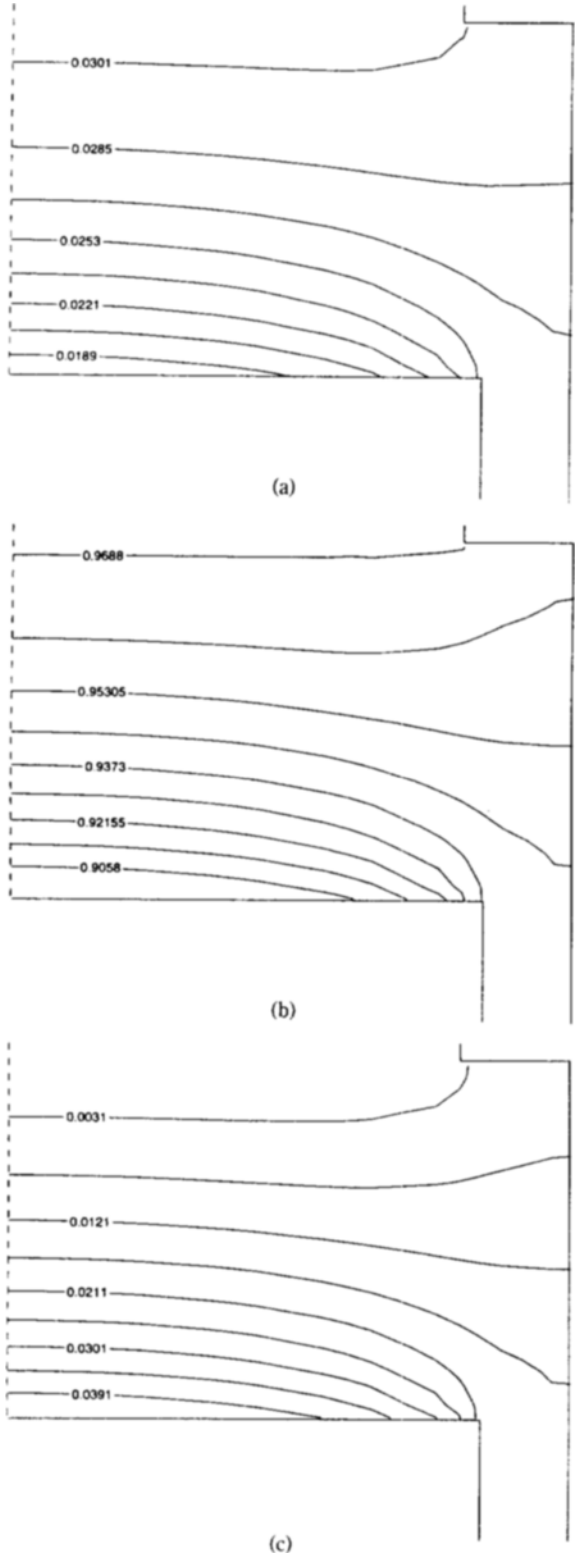


**Fig. 4. Contours of mole fractions of a. $WF_6$, b. DCS, c. HCl.**

to that in the feed stream decrease with increasing temperature. The differences in these ratios between at the wafer center and at the wafer edge increase with increasing temperature. Fig. 7 shows the average deposition rate and deposition rate nonuniformity as functions of wafer temperature. Deposition rate and deposi-

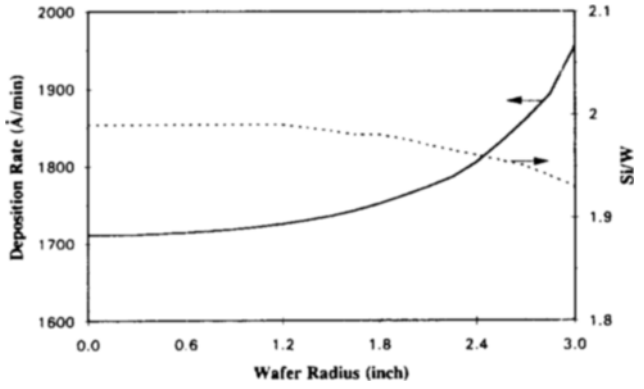


Fig. 5. Deposition rate and the ratio of silicon to tungsten as functions of wafer radial position. The wafer temperature is 763 K, the total pressure is 0.18 torr, the flow rate of DCS is 120 sccm and the flow rate of $WF_6$ is 3.8 sccm.

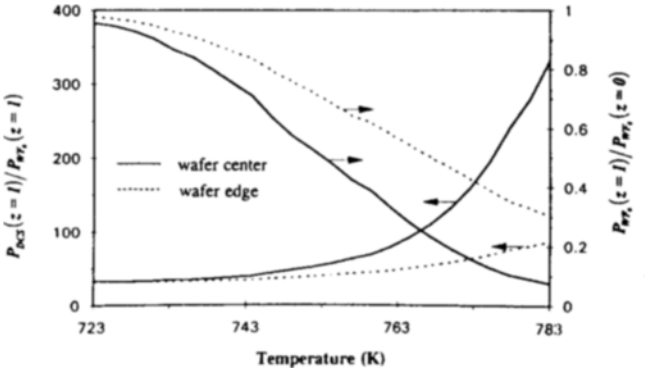


Fig. 6. Ratio of the $WF_6$ partial pressure at the wafer surface to the $WF_6$ partial pressure at the reactor inlet as a function of wafer temperature and ratio of DCS and $WF_6$ partial pressures at the wafer center as a function of wafer temperature.

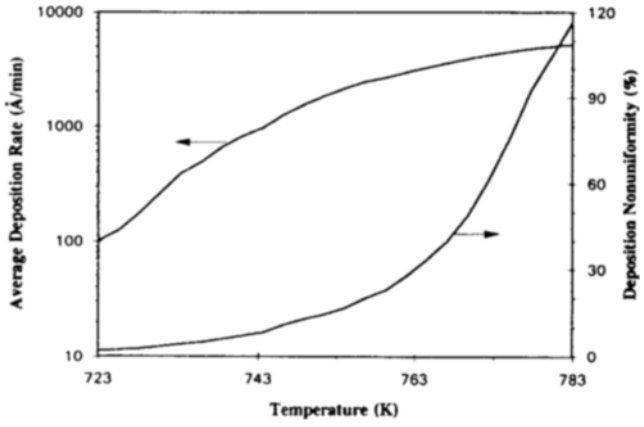


Fig. 7. Average deposition rate and deposition nonuniformity as functions of wafer temperature.

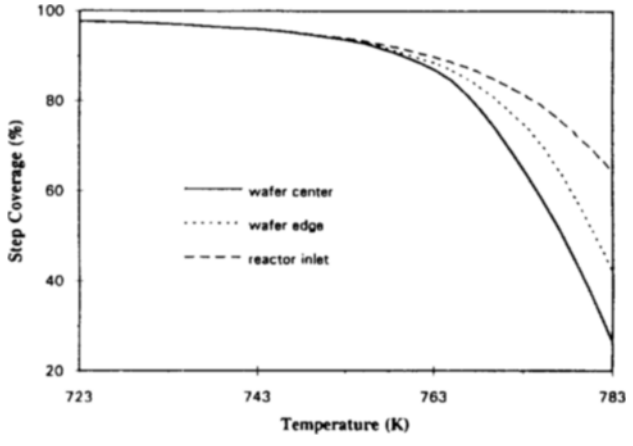


Fig. 8. Step coverages predicted using inlet partial pressures and partial pressures at the wafer center and wafer edge as functions of wafer temperature. The initial aspect ratio of trench used is 1.

tion nonuniformity usually increase with increasing temperature. Nonuniformity is defined in this work as

$$\Delta = [F(r = \text{wafer edge}) - F(r = 0)]/F(r = 0). \quad (28)$$

Significant deposition nonuniformity occurs above 755 K of temperature. However, the change in temperature does not significantly affect composition uniformity.

Even without solving the model equations, several useful "rules of thumb" for improving step coverage in LPCVD processes can be predicted [Cale and Raupp, 1990; Cale et al., 1991b]. Essentially, step coverage increases with decreasing step coverage modulus at constant partial pressure ratio. Using the step coverage modulus as a guideline, the following parameter adjustment may be used to decrease step coverage modulus: (i) decrease the feature height or reaction rate, (ii) increase the feature width at constant reactant concentrations. During deposition process, achieving good film conformality in features and good step coverage uniformity across the wafer is important [Cale et al., 1993]. Step coverage predictions for the DRM depend on knowing the local reactant concentrations and the wafer temperature, which can be obtained using the RSM. Fig. 8 shows step coverages predicted using the partial pressures at the reactor inlet and those at the wafer surface as functions of wafer temperature. Step coverage (film conformality in features) is defined as the ratio of the deposited thickness of the side-wall at the bottom of the feature to the deposited thickness at the feature mouth at the time when the feature mouth is completely filled. Long infinite trenches having initial aspect ratio of 1 (1 μm×1 μm) are used before tungsten silicide deposition starts. In these results, the partial pressures of DCS and $WF_6$ at the trench mouth are calculated by the RSM with varying the temperature. Step coverages calculated by the feed partial pressures are substantially higher than those predicted by the partial pressures at the wafer surface above 760 K of wafer temperature. The differences in step coverage predicted by the feed partial pressure and the partial pressures at the wafer surface are more significant at higher temperatures. On the other hand, step coverage is the same below 753 K, even though any deposition conditions are used. The reason is that the conversion of the reactants is considerably low at lower temperatures. In addition to the dependence of step coverage in trenches on operating conditions of the reactor, significant differences in step coverage across a wafer are also observed. For the operating conditions and reactor dimensions considered in this study, the step

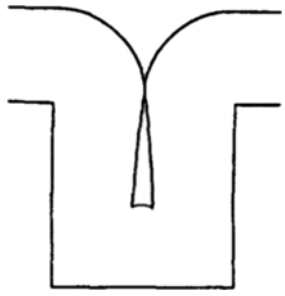

**Fig. 9. Final film profile of trench of aspect ratio of one for a wafer temperatre of 763 K.**

coverage at the wafer center is lower than that at the wafer edge, although the deposition rate and reactant concentrations are actually lower at the wafer center. This degradation in step coverage results from the higher values of partial pressure ratio $\Lambda_{CF}$ at the wafer center relative to those at the wafer edge, as shown in Fig. 6. The differences in step coverage across the wafer increase with increasing the temperature. Fig. 9 shows final film profile for tungsten silicide in a trench of aspect ratio of one for a wafer temperature of 763 K. The reactant partial pressures at the wafer center are obtained by the reactor scale model. The resulting step coverage is 88% at feature mouth closure. From a processing view point, higher step coverage is desirable. To enhance step coverage on patterned wafers and step coverage uniformity across the wafer, the temperature and the partial pressure ratio DCS to $WF_6$ in the feed should be decreased.

## CONCLUSIONS

A transient, stagnation point flow, single-wafer RSM is combined during LPCVD of tungsten silicide to demonstrate deposition uniformity and step coverage uniformity across the wafer and film composition. The RSM predicts reactant concentrations and deposition rates as functions of position on the wafer surface. These concentrations are used in the DRM to predict conformality.

The DRM is used in this study to provide insight into the effect of operating conditions on step coverage. Different step coverages at radial positions on the wafer were observed in terms of reactor operating conditions. An assumption of no conversion of reactants in the reactor scale which is often used for the feature scale model can cause significant errors in prediction of step coverage. In the absence of the RSM solution, therefore, some considerations should be made in determination of reactant concentrations by accounting for the conversion of the reactants for the feature scale model.

The use of a combined RSM and feature scale model presented was used to provide qualitative guidance regarding how to change operating conditions to improve uniformities of film properties. The same approach can be used to optimize operating conditions for other deposition processes; e.g., atmospheric pressure CVD processes in MWRs, assuming that validated reactor and feature scale models are available.

## ACKNOWLEDGMENTS

The author gratefully acknowledges the Semiconductor Research Corporation and National Science Foundation, U.S.A., for this work. The author is also grateful for assistance by Dr. T. S. Cale.

**Table 2. Values for intermolecular force constants**

| Species | $\sigma$ (Å) | $(\varepsilon/\kappa)$ (K) |
|---|---|---|
| HCl | 3.339 | 344.7 |
| $SiF_4$ | 4.880 | 171.9 |
| $WF_6$ | 5.134 | 342.0 |
| $SiH_2Cl_2$ | 5.027 | 332.1 |
| $SiF_2$ | 4.289 | 447.0 |

**Table 3. Values for coefficients in Eq. (A.5) for heat capacity (cal/mol K)**

| Species | $\alpha$ | $\beta$ | $\gamma$ |
|---|---|---|---|
| HCl | 6.878 | $-4.320\cdot10^{-5}$ | $7.027\cdot10^{-7}$ |
| $SiF_4$ | 12.345 | $2.401\cdot10^{-2}$ | $-1.226\cdot10^{-5}$ |
| $WF_6$ | 22.074 | $3.022\cdot10^{-2}$ | $-1.600\cdot10^{-5}$ |
| $SiH_2Cl_2$ | 8.159 | $2.713\cdot10^{-2}$ | $-1.283\cdot10^{-5}$ |
| $SiF_2$ | 7.810 | $1.177\cdot10^{-2}$ | $-6.267\cdot10^{-6}$ |

## APPENDIX

The viscosity of gaseous species in g/(cm·sec) is calculated using the Chapman-Enskog theory [Reid et al., 1988]

$$\mu_i = 2.6693\times10^{-5}\frac{\sqrt{m_i T}}{\sigma_i^2\Omega_{\mu i}} \tag{A.1}$$

where $\sigma_i$ is the collision diameter in Angstrom and the collision integral $\Omega_{\mu i}$ is defined by

$$\Omega_{\mu i} = \frac{1.1645}{T_i^{*0.14874}} + \frac{0.52487}{\exp(0.7732T_i^*)} + \frac{2.16178}{\exp(2.43787T_i^*)} \tag{A.2}$$

where $T_i^* = T(\kappa/\varepsilon)_i$. Values of $\sigma$ and $\varepsilon/\kappa$ for each species in this system are summarized in Table 2. Values for HCl and $SiF_4$ are obtained from Svehla [1962], and values for $WF_6$, DCS and $SiF_2$ are estimated [Park, 1992]. The viscosity of the gas mixture is computed from Wilke's formula, *viz.*

$$\mu_m = \sum_{i=1}^{n}\left(\frac{x_i\mu_i}{\sum_{j=1}^{n} x_j\Phi_{ij}}\right) \tag{A.3}$$

with

$$\Phi_{ij} = \frac{1}{\sqrt{8}}\left(1+\frac{m_i}{m_j}\right)^{-1/2}\left[1+\left(\frac{\mu_i}{\mu_j}\right)^{1/2}\left(\frac{m_j}{m_i}\right)^{1/4}\right]^2. \tag{A.4}$$

The heat capacity for each species i is described by

$$c_{pi} = \alpha_i + \beta_i T + \gamma_i T^2. \tag{A.5}$$

Values for coefficients in Eq. (A.5), which are available [Chase et al., 1985; Pankratz, 1984], are given in Table 3. The specific heat of the gas mixture is calculated by

$$c_{pm} = \sum_{i=1}^{n}\omega_i(c_{pi}/m_i). \tag{A.6}$$

The thermal conductivity of atomic gases is estimated by Eucken's correlation [Reid et al., 1988].

$$\lambda_i = \left(c_{pi} + \frac{5}{4}R_g\right)\frac{\mu_i}{m_i} \tag{A.7}$$

The thermal conductivity of the gas mixture is computed by an expression analogous to Eq. (A.3).

The binary diffusion coefficients are calculated using the Chapman-Enskog theory [Reid et al., 1988]

$$D_{ij} = 0.0018583\,\frac{\sqrt{T^3(1/m_i + 1/m_j)}}{P\,\sigma_{ij}^2\Omega_{D,ij}} \tag{A.8}$$

where $\sigma_{ij} = (\sigma_i + \sigma_j)/2$ and $(\varepsilon/\kappa)_{ij} = \sqrt{(\varepsilon/\kappa)_i(\varepsilon/\kappa)_j}$. The collision integral $\Omega_{D,ij}$ is analogous to that used in Eq. (A.2), *viz.*

$$\Omega_{D,ij} = \frac{1.06036}{T_{ij}^{*0.15610}} + \frac{0.19300}{\exp(0.47635T_{ij}^*)} + \frac{1.03587}{\exp(1.52995T_{ij}^*)} + \frac{1.76474}{\exp(3.89411T_{ij}^*)} \tag{A.9}$$

with $T_{ij}^* = T(\kappa/\varepsilon)_{ij}$. The diffusion coefficient of species i in a multicomponent mixture is calculated by Wilke's approximation

$$D_{im} = (1 - x_i)\left(\sum_{\substack{j=1 \\ j\neq i}}^{n} \frac{x_j}{D_{ij}}\right). \tag{A.10}$$

Multicomponent thermal diffusion coefficients are calculated using the kinetic theory of gases based on the Lennard-Jones potential [Hirschfelder et al., 1954; Park, 1992].

Local Knudsen diffusivities for infinitely long trenches are estimated by [Cale et al., 1990].

$$D_{Ki} = \left(\frac{8\kappa T}{\pi m_i}\right)^{1/2}\frac{h(t)}{4}\left[\frac{18 + 7\{h(t)/w(x,t)\}}{18 + 16\{h(t)/w(x,t)\} + 2\{h(t)/w(x,t)\}^2}\right]. \tag{A.11}$$

## NOMENCLATURE

- c : molar concentration [mol/cm$^3$]
- $c_{pi}$ : molar heat capacity of species i [cal/mole K]
- $c_{pm}$ : heat capacity of mixture [cal/g K]
- $D_{ij}$ : diffusivity of binary species [cm$^2$/sec]
- $D_{im}$ : diffusivity of species i in a multicomponent mixture [cm$^2$/sec]
- $D_{Ki}$ : Knudsen diffusivity of species i [cm$^2$/sec]
- $\mathcal{B}_i$ : dimensionless Knudsen diffusivity of species i, $D_{Ki}(x,t)/D_{Ki}(0,0)$
- $D_i^T$ : thermal diffusion coefficient of species i [g cm/sec]
- $E_a$ : activation energy in rate expression [cal/mol]
- F : deposition rate [Å/min]
- **g** : gravitational acceleration vector [cm/sec$^2$]
- $G_j$ : dimensionless rate of surface reaction j, $\mathfrak{R}_j(x,t)/\mathfrak{R}_j(0,0)$
- h : feature depth [cm]
- H : dimensionless feature depth, h(t)/h(0)
- **I** : identity vector
- $k_0$ : pre-exponential factor in rate expression
- $K_j$ : adsorption coefficient of $WF_6$ for surface reaction j (torr$^{-1}$)
- $l$ : number of solid phase species
- $m_i$ : molecular weight of species i [g/mol]
- $m_s$ : molecular weight of solid [g/mol]
- n : number of gas phase species
- p : partial pressure [torr]
- P : total pressure [atm]
- r : radial coordinate [cm]
- $R_g$ : universal gas constant [atm cm$^3$/mol K, or cal/mol K]
- $\mathfrak{R}$ : surface reaction rate [mol/cm$^2$ sec]
- t : time [sec]
- T : temperature [K]
- T* : reduced temperature, $\kappa T/\varepsilon$
- **v** : mass average velocity vector [cm/sec]
- $v_r$ : gas velocity in the radial direction [cm/sec]
- $v_z$ : gas velocity in the axial direction [cm/sec]
- w : feature width [cm]
- W : dimensionless feature width, w(x,t)/w(0,0)
- x : coordinate into trench [cm]
- $x_i$ : mole fraction of species i
- z : axial coordinate [cm]

### Greek Letters

- $\alpha_0$ : initial aspect ratio in a trench, h(0)/w(0,0)
- $\delta_j$ : parameter used in Eq. (20), $\rho_{s,j}/m_{s,j}c_r(0,0)$ (j=1 for Si, j=2 for $WSi_2$, j=3 for $W_5Si_3$)
- $\Delta$ : deposition nonuniformity
- $\varepsilon$ : Lennard-Jones potential energy between two molecules [g cm$^2$/sec$^2$]
- $\phi_j$ : step coverage modulus for reaction j, $2h^2(0)\mathfrak{R}_j(0,t)/w(0,0)c_C(0,0)D_{KC}(0,0)$
- $\Phi_{ij}$ : function defined by Eq. (A.4)
- $\Gamma$ : parameter defined in Eq. (21), $D_{KF}(0,0)/D_{KC}(0,0)$
- $\kappa$ : Boltzmann's constant ($=3.30\times10^{-24}$ cal/K)
- $\Lambda_{ij}$ : partial pressure ratio at the wafer surface, $p_i/p_j$
- $\lambda_i$ : thermal conductivity of species i [cal/cm sec K]
- $\lambda_m$ : thermal conductivity of mixture [cal/cm sec K]
- $\mu_i$ : viscosity of species i [g/cm sec]
- $\mu_m$ : viscosity of mixture [g/cm sec]
- $\nu_{ij}$ : stoichiometric coefficient of species i for reaction j
- $\theta_i$ : dimensionless concentration of species i, $c_i(x,t)/c_i(0,0)$
- $\rho$ : fluid density [g/cm$^3$]
- $\rho_s$ : solid phase density [g/cm$^3$]
- $\Theta$ : parameter defined in Eq. (24), $c_C(0,0)D_{KC}(0,0)/c_F(0,0)D_{KF}(0,0)$
- $\sigma$ : collision diameter for the Lennard-Jones parameter [Å]
- $\tau$ : dimensionless time for the DRM, $tD_{KC}(0,0)/h^2(0)$
- $\xi$ : dimensionless distance into trench, x/h(t)
- $\omega_i$ : mass fraction of species i
- $\Omega_D$ : collision integral defined in Eq. (A.9)
- $\Omega_\mu$ : collision integral defined in Eq. (A.2)

### Superscripts

- t : transpose
- T : thermal diffusion

### Subscripts

- 0 : reactor inlet
- C : dichlorosilane
- F : tungsten hexafluoride
- i : index
- j : index
- k : index
- K : Knudsen
- m : mixture
- s : susceptor
- w : wall

### Acronyms

BTRM : ballistic transport-reaction model
CVD : chemical vapor deposition
DCS : dichlorosilane
DRM : diffusion-reaction model
LPCVD : low pressure chemical vapor deposition
MWR : multiple-wafer reactor
OCFE : orthogonal collocation on finite elements
ODE : ordinary differential equation
RSM : reactor scale model
SWR : single-wafer reactor

## REFERENCES


Bullis, W. M. and O'Mara, W. C., "Large-Diameter Silicon Wafer Trends", *Solid State Technol.*, **36**(4), 59 (1993).

Cale, T. S., Park, J.-H., Gandy, T. H., Raupp, G. B. and Jain, M. K., "Step Coverage Predictions Using Combined Reactor Scale and Feature Scale Models for Blanket Tungsten LPCVD", *Chem. Eng. Comm.*, **119**, 197 (1993).

Cale, T. S., Park, J. H., Raupp, G. B., Jain, M. K. and Rogers, B. R., "The Inherently Transient Nature of Deposition Processes", in Advanced Metallization for ULSI Applications, Rana, V. V. S., Joshi, R. V. and Ohdomari, I., eds., MRS, Pittsburg, p. 93 (1992a).

Cale, T. S., Raupp, G. B., Park, J. H., Jain, M. K. and Rogers, B. R., "The Inherently Transient Nature of Deposition Processes", in Proceedings of First International Conference of Transport Phenomena in Processing, Guceri, S., ed., Technomic Publishing Co., p. 127 (1992b).

Cale, T. S., Park, J. H., Raupp, G. B. and Jain, M. K., "Impacts of Temperature and Reactant Flow Rate Transients on LPCVD Tungsten Silicide Film Properties", in Rapid Thermal and Integrated Processing, Mat. Res. Soc. Symp. Proc., Vol. 224, MRS, p. 171 (1991a).

Cale, T. S., Gandy, T. H. and Raupp, G. B., "A Fundamental Feature Scale Model for Low Pressure Deposition Processes", *J. Vac. Sci. Technol.*, **A9**(3), 524 (1991b).

Cale, T. S., Jain, M. K. and Raupp, G. B., "Programmed Rate Processing to Increase Throughput in LPCVD", *J. Electrochem. Soc.*, **137**(5), 1526 (1990).

Cale, T. S. and Raupp, G. B., "A Unified Line-of Sight Model for Deposition in Rectangular Vias", *J. Vac. Sci. Technol.*, **B8**(6), 1242 (1990).

Campbell, S. A., Knutson, K. L., Ahn, K. H., Leighton, J. D. and Liu, B., "Gas Flow Patterns and Thermal Uniformity in Rapid Thermal Processing Equipment", IEEE IEDM Technical Digest, p. 921 (1990).

Chase, Jr., M. W., Davies, C. A., Downey, Jr., J. R., Frurip, D. J., McDonald, R. A. and Syverud, A. N.: "JANAF Thermochemical Tables", *J. Phys. Chem. Ref. Data*, Vol. 14, 1985.

Chatterjee, S., Trachtenberg, I. and Edgar, T. F., "Mathematical Modeling of a Single-Wafer Rapid Reactor", *J. Electrochem. Soc.*, **139**(12), 3682 (1992).

Chatterjee, S. and McConica, C. M., "Prediction of Step Coverage during Blanket CVD Tungsten Deposition in Cylinder Pores", *J. Electrochem. Soc.*, **137**(1), 328 (1990).

Dobkin, D. M., "Kinetics and Uniformity of Deposition of Borophosphosilicate Glass from Silane and Oxygen in a Single-Wafer Reactor", *J. Electrochem. Soc.*, **139**(9), 2573 (1992).

Economou, D. J. and Alkire, R. C., "A Mathematical Model for a Parallel Plate Plasma Etching Reactor", *J. Electrochem. Soc.*, **135** (11), 2786 (1988).

Finlayson, B. A.: "Nonlinear Analysis in Chemical Engineering", McGraw-Hill Inc., New York, 1980.

Fitzjohn, J. L. and Holstein, W. L., "Divergent Flow in Chemical Vapor Deposition Reactors", *J. Electrochem. Soc.*, **137**(2), 699 (1990).

Hirschfelder, J. O., Curtiss, C. F. and Bird, R. B.: "Molecular Theory of Gases and Liquids", John Wiley & Sons, Inc., 1954.

IslamRaja, M. M., Capelli, M. A., McVittie, J. P. and Saraswat, K. C., "A 3-Dimensional Model for Low Pressure Chemical Vapor Deposition Step Coverage in Trenches and Circular Vias", *J. Appl. Phys.*, **70**(11), 7137 (1991).

Jain, M. K., Cale, T. S. and Gandy, T. H., "Comparison of LPCVD Film Conformalities Predicted by Ballistic Transport-Reaction and Continuum Diffusion-Reaction Models", *J. Electrochem. Soc.*, **140**(1), 242 (1993).

Jasinski, T. J. and Kang, S. S., "Application of Numerical Modeling for CVD Simulation Test Case: Blanket Tungsten Deposition Uniformity", Tungsten and Other Advanced Metals for ULSI Applications in 1990, Smith, G. C. and Blumenthal, R., eds., MRS, Pittsburg, p. 129 (1991).

Jenkinson, J. P. and Pollard, R., "Thermal Diffusion Effects in Chemical Vapor Depositon Reactors", *J. Electrochem. Soc.*, **131** (12), 2911 (1984).

Kleijn, C. R., van der Meer, Th. H. and Hoogendoorn, C. J., "A Mathematical Model LPCVD in a Single Wafer Reactor", *J. Electrochem. Soc.*, **136**(11), 3423 (1989).

Kleijn, C. R., Hoogendoorn, C. J., Hasper, A., Holleman, J. and Middelhock, J., "Transport Phenomena in Tungsten LPCVD in a Single-Wafer Reactor", *J. Electrochem. Soc.*, **138**(2), 509 (1991).

Kleijn, C. R., "A Mathematical Model of the Hydrodynamics and Gas-Phase Reactions in Silicon LPCVD in a Single-Wafer Reactor", *J. Electrochem. Soc.*, **138**(7), 2190 (1991).

Lam, D. K. and Koch, G. R., "Vacuum System Considerations for Plasma Etching Equipment", *Solid State Technol.*, **23**(9), 99 (1980).

McConica, C. M., Chatterjee, S. and Sivaram, S., "Step Coverage Prediction During Blanket LPCVD Tungsten Deposition from Hydrogen, Silane and Tungsten Hexafluoride", in Fifth Annual IEEE VLSI Multilevel Interconnection Conference, Santa Clara, CA, June, p. 268 (1988).

Moslehi, M. M., Chapman, R. A., Wong, M., Paranjpe, A., Najm, H. N., Kuehne, J., Yeakley, R. L. and Davis, C. J., "Single-Wafer Integrated Semiconductor Device Processing", IEEE Trans. Electron Devices, **ED-39**(1), 4 (1992).

Netlib Contains Many Source Codes Served by AT&T Bell Labs in Murray Hill, N.J., U.S.A.

Pankratz, L. B., "Thermodynamics Properties of Halides", U.S. Bureau of Mines, Bulletin 674, 1984.

Park, S.-K. and Economou, D. J., "Numerical Simulation of a Single-Wafer Isothermal Plasma Etching Reactor", *J. Electrochem. Soc.*, **137**(8), 2624 (1990).

Park, J.-H., "Simulation of Low Pressure Chemical Vapor Deposition Using Combined Reactor Scale and Feature Scale Models", Ph D. Dissertation, Arizona State University, U.S.A., 1992.

Raupp, G. B. and Cale, T. S., "Step Coverage Prediction in Low-Pressure Chemical Vapor Deposition", *Chemistry of Materials*, **1**, 207 (1989).

Raupp, G. B., Cale, T. S., Jain, M. K., Rogers, B. and Srinivas, D., "Step Coverage of Tungsten Silicide Films Deposited by Low Pressure Dichlorosilane Reduction of Tungsten Hexafluoride", *Thin Solid Films*, **193**, 234 (1990).

Reid, R. C., Prausnitz, J. M. and Poling, B. E., "The Properties of Gases & Liquids", McGraw-Hill, Inc., New York, 1988.

Riely, P. E. and Clark, T. E., "Integrated Chemical Vapor Deposition and Plasma Etchback of Tungsten in Multichamber, Single-Wafer System", *J. Electrochem. Soc.*, **138**(10), 3008 (1991).

Rode, E. J. and Schmitz, J. E. J., "Study of Reactor Design by Computational Fluid Dynamics", in Advanced Metallization for ULSI Applications, Rana, S., Joshi, R. V. and Ohdomari, I., eds., MRS, Pittsburg, p. 105 (1992).

Suwondo, E., Pibouleau, L., Domenech, S. and Riba, J. P., "Simulation Via Orthogonal Collocation on Finite Element of a Chromatographic Column with Nonlinear Isotherm", *Chem. Eng. Comm.*, **102**, 161 (1991).

Svehla, R. A., "Estimated Viscosities and Thermal Conductivities of Gases at High Temperatures", NASA Tech. Report R-132, Lewis Res. Center, Cleveland, OH, 1962.

Ulacia, F., Howell, J. I., Krner, H. and Werner. Ch., "Flow and Reaction Simulation of a Tungsten CVD Reactor", *Appl. Sur. Sci.*, **38**, 370 (1989).

Wong, F., "Single-Wafer RTP-CVD Epitaxial Deposition Technology", *Solid State Technol.*, **32**(10), 53 (1989).